Parity symmetry as the origin of 'spin' in the quantum spin Hall effect

Wouter Beugeling ◉[*]

Experimentelle Physik III, Physikalisches Institut, Universität Würzburg, Am Hubland, 97074 Würzburg, Germany
and Institute for Topological Insulators, Am Hubland, 97074 Würzburg, Germany

The quantum spin Hall effect arises due to band inversion in topological insulators, and has the defining characteristic that it hosts helical edge channels at zero magnetic field, leading to a finite spin Hall conductivity. The spin Hall conductivity is understood as the difference of the contributions of two spin states. In the effective four-band Bernevig-Hughes-Zhang model, these two spin states appear as two uncoupled blocks in the Hamiltonian matrix. However, this idea breaks down if additional degrees of freedom are considered. The two blocks cannot be identified by proper spin S_z or total angular momentum J_z, both not conserved quantum numbers. In this work, we discuss a notion of block structure for the more general $\mathbf{k} \cdot \mathbf{p}$ model, defined by a conserved quantum number that we call *isoparity*, a combination of parity $z \to -z$ and spin. Isoparity remains a conserved quantity under a wide range of conditions, in particular in presence of a perpendicular external magnetic field. From point-group considerations, isoparity is fundamentally defined as the action of $z \to -z$ on the spatial and spinorial degrees of freedom. Since time reversal anticommutes with isoparity, the two blocks act as Kramers partners. The combination of conductivity and isoparity defines spin conductivity. This generalized notion of spin Hall conductivity uncovers the meaning of 'spin': It is not the proper spin S_z, but a crystal symmetry that is realized by a spinorial representation.

I. INTRODUCTION

The experimental realization [1,2] and theoretical prediction [3,4] of the quantum spin Hall effect have initiated a huge interest in the physics of topological insulators in the past two decades. As opposed to the quantum Hall effect, that is generated by an external magnetic field [5], the quantum spin Hall effect is rooted in the intrinsic band inversion of the material [1,4]. The quantum spin Hall effect is tied to time-reversal symmetry: In the absence of an external magnetic field, the Hall conductance vanishes, but at the same time the system hosts a pair of counterpropagating edge channels, giving rise to so-called spin Hall conductance [4]. In practice, these counterpropagating edge channels can be observed as a quantized longitudinal conductance $G = 2e^2/h$ in the absence of a magnetic field [1,6].

The mechanism of band inversion giving rise to helical edge channels has been elegantly explained in the model proposed by Bernevig, Hughes, and Zhang (BHZ) [4]. In order to explain the transition from trivial to topological behavior in HgTe/(Hg,Cd)Te quantum wells at the critical thickness $d_c = 6.3$ nm, it is sufficient to project the Hamiltonian to the subspace of the four subbands $|E1, \pm\rangle$ and $|H1, \pm\rangle$, the spin-degenerate pairs of the first subband in both the conduction and valence bands. The two spin states are uncoupled, so that the 4×4 matrix Hamiltonian splits into two 2×2 blocks [4].

The BHZ model is obtained by an expansion of the Hamiltonian near the Γ point projected to the four subband states

of its basis. It is extracted from $\mathbf{k} \cdot \mathbf{p}$ models which contain many more degrees of freedom and describe more aspects of the band structure in an accurate manner [7–11]. The four-band BHZ model is unable to capture physics where these other degrees of freedom are essential. For example, it does not predict the dispersion of the *camel back*, a maximum in the dispersion of the valence band at finite momentum, that arises due to hybridization of the E1 subband with higher-order heavy-hole subbands like H2 [12,13]. The camel back can play a dominant role in the transport properties of HgTe quantum wells of thickness $d \gtrsim 7$ nm, already quite close to d_c. A proper description thus requires band structures obtained from the $\mathbf{k} \cdot \mathbf{p}$ model [13] or from extended BHZ models with more than four subbands [14].

The necessity of considering these more advanced models motivates the question whether they admit a similar block structure as the four-band BHZ model. Extended BHZ models do, but the grouping of the subbands is not entirely intuitive: The subband $|H2, +\rangle$ couples with $|E1, -\rangle$ and $|H1, -\rangle$ [14], where the label $\pm$ refers to $\langle \text{sgn}(J_z) \rangle$, where J_z is total angular momentum with quantization axis along the growth direction z. This example shows that the blocks are not defined by spin only, but by a combination of spin and parity: the envelope function $g(z)$ of $|H2, \pm\rangle$ is odd under parity $z \to -z$, whereas that of $|H1, \pm\rangle$ is even [15]. The idea of a discrete symmetry that acts on spin and parity $z \to -z$ simultaneously extends to the $\mathbf{k} \cdot \mathbf{p}$ model as well [16].

In this work, we elaborate on the role of the combination of parity and spin, called *isoparity* $\tilde{\mathcal{P}}_z$, in defining a block structure in the $\mathbf{k} \cdot \mathbf{p}$ model in the inversion-symmetric approximation [17]. Isoparity is a conserved quantity with respect to the $\mathbf{k} \cdot \mathbf{p}$ Hamiltonian H_k (i.e., $[H_k, \tilde{\mathcal{P}}_z] = 0$) even

*wbeugeling@physik.uni-wuerzburg.de

at finite momentum, unlike spin S_z and total angular momentum J_z. Uniaxial strain, encoded by the Pikus-Bir strain Hamiltonian [10,18], and couplings with the magnetic fields in the perpendicular direction ($\mathbf{B} \parallel \hat{z}$) also preserve isoparity. While isoparity is not conserved if the symmetry $z \rightarrow -z$ is broken by, e.g., a perpendicular electric field (gate voltage) or in an asymmetric geometry like a type-II topological insulator device [19], it can be convenient to define the basis in terms of isoparity eigenstates; the inversion-asymmetric terms then appear in the off-diagonal block, analogous to the structure known in the context of the BHZ model [15,19].

From analysis of the representations of the relevant double point group (in the inversion-symmetric model, $\tilde{O}_h$ or $\tilde{D}_{4h}$ for bulk and quantum well geometry, respectively), we confirm that isoparity is identical to the mirror transformation m_z in the z direction, up to the imaginary factor i. The blocklike structure of the Hamiltonian, given by invariance under isoparity, is thus fundamentally a consequence of crystal symmetry. By identifying the action of time reversal in the context of representation theory, we show that isoparity and time reversal anticommute. Time reversal thus maps one block to the other. Importantly, this relation proves that the two blocks are Kramers partners, establishing it as generalization of this idea known from the BHZ model [4]. The combination of the ordinary conductance tensor σ_{ij} with isoparity yields the spin conductance $\tilde{\sigma}_{ij}$. By construction, spin conductance is odd under time reversal, unlike ordinary conductance which is even; these properties are dictated by crystal and time-reversal symmetry as well as Onsager's relation [20,21]. This difference is related to the fundamentally different origins of the Hall effect and spin Hall effect, respectively [22].

With these ingredients, we establish an unambiguous interpretation of the word 'spin' in "quantum spin Hall effect": It does not indicate proper spin S_z, which is not a conserved quantum number, but it refers to the crystal symmetry m_z. The name 'spin' is appropriate nevertheless, as it involves an operation that is inherently spinlike in nature, namely, it acts according to a spin representation onto the half-integer angular momentum degrees of freedom and it anticommutes with time reversal.

The outline of the paper is as follows. In Sec. II, we briefly introduce our model, with further details in the Appendix. In Sec. III, we provide the ideas of the splitting into blocks in more detail, and define isoparity based on those observations. We then prove that isoparity is invariant, and how external effects (magnetic, electric, and strain couplings) affect this invariance. In Sec. IV, we interpret isoparity in the context of spin representations of the point group. We discuss time reversal in Sec. V. The notions of conductivity and spin conductivity are defined and analyzed in Sec. VI. The concluding Sec. VII discusses some practical applications and implications for the interpretation of the term 'spin' in this framework.

II. MODELING

As the basis for our analysis, we use the eight-orbital $\mathbf{k} \cdot \mathbf{p}$ model for (Hg,Cd)Te and (Hg,Mn)Te presented in

Refs. [8–10] as a starting point. The eight-orbital basis is

$$|\Gamma_6, +\tfrac{1}{2}\rangle = |S\rangle \otimes |\uparrow\rangle,$$
$$|\Gamma_6, -\tfrac{1}{2}\rangle = |S\rangle \otimes |\downarrow\rangle,$$
$$|\Gamma_8, +\tfrac{3}{2}\rangle = \tfrac{1}{\sqrt{2}}|X + iY\rangle \otimes |\uparrow\rangle,$$
$$|\Gamma_8, +\tfrac{1}{2}\rangle = \tfrac{1}{\sqrt{6}}(|X + iY\rangle \otimes |\downarrow\rangle - 2|Z\rangle \otimes |\uparrow\rangle),$$
$$|\Gamma_8, -\tfrac{1}{2}\rangle = \tfrac{1}{\sqrt{6}}(-|X - iY\rangle \otimes |\uparrow\rangle - 2|Z\rangle \otimes |\downarrow\rangle),$$
$$|\Gamma_8, -\tfrac{3}{2}\rangle = -\tfrac{1}{\sqrt{2}}|X - iY\rangle \otimes |\downarrow\rangle,$$
$$|\Gamma_7, +\tfrac{1}{2}\rangle = \tfrac{1}{\sqrt{3}}(|X + iY\rangle \otimes |\downarrow\rangle + |Z\rangle \otimes |\uparrow\rangle),$$
$$|\Gamma_7, -\tfrac{1}{2}\rangle = \tfrac{1}{\sqrt{3}}(|X - iY\rangle \otimes |\uparrow\rangle - |Z\rangle \otimes |\uparrow\rangle), \quad (1)$$

in terms of the s orbital labeled S and the p orbitals labeled X, Y, and Z, as well as the two spin states $\uparrow$ and $\downarrow$. For convenience of notation, we split the Hamiltonian H into orbital blocks H_{pq} with $p, q = 6, 7, 8$ labeling the orbital sectors $|\Gamma_p, \cdot\rangle$:

$$H = \left(\begin{array}{c|c|c} H_{66} & H_{68} & H_{67} \\ \hline H_{86} & H_{88} & H_{87} \\ \hline H_{76} & H_{78} & H_{77} \end{array} \right). \quad (2)$$

Hermiticity of H implies that $H_{qp} = H_{pq}^{\dagger}$. Our investigation will mostly be targeted at the inversion-symmetric part of the $\mathbf{k} \cdot \mathbf{p}$ Hamiltonian, denoted H_k. The blocks of H_k are given in Appendix A, together with the matrix representations of spin S_i and total angular momentum J_i ($i = x, y, z$). Strain, magnetic and electric couplings, as well as inversion-asymmetric terms will be discussed separately.

III. SPIN, PARITY, ISOPARITY

A. Incentive

The Hamiltonian H_k preserves neither spin S_z nor total angular momentum J_z,

$$[H_k, S_z] \neq 0, \quad [H_k, J_z] \neq 0, \quad (3)$$

for $\mathbf{k} \neq 0$. This can be demonstrated straightforwardly by examining the eigenstate expectation values $\langle S_z \rangle$ and $\langle J_z \rangle$ in a typical quantum well dispersion, e.g., for 7-nm-thick HgTe between (Hg,Cd)Te barriers, as illustrated in Fig. 1. In Figs. 1(a) and 1(b), we have plotted the dispersion with the coloring based on the expectation values $\langle S_z \rangle$ and $\langle J_z \rangle$, respectively. The curves not being uniformly colored indicates that these expectation values are momentum dependent. Thus, S_z and J_z do not define good quantum numbers.

The widespread terminology "spin-up" and "spin-down" states (with notation typically $+$ and $-$, respectively, sometimes $\uparrow$ and $\downarrow$, respectively) is typically understood in the sense $J_z > 0$ and $J_z < 0$; the word 'spin' should be read as 'pseudospin.' Whereas this is an intuitive and workable definition in some limited contexts, in particular in the four-band BHZ model [4], it can be problematic in other cases that require consideration of more degrees of freedom. First, for large in-plane momentum (k_x, k_y), hybridization may occur between subbands, e.g., between the subbands labeled E1 and H2 in Fig. 1, leading to the typical camel-back feature [13].
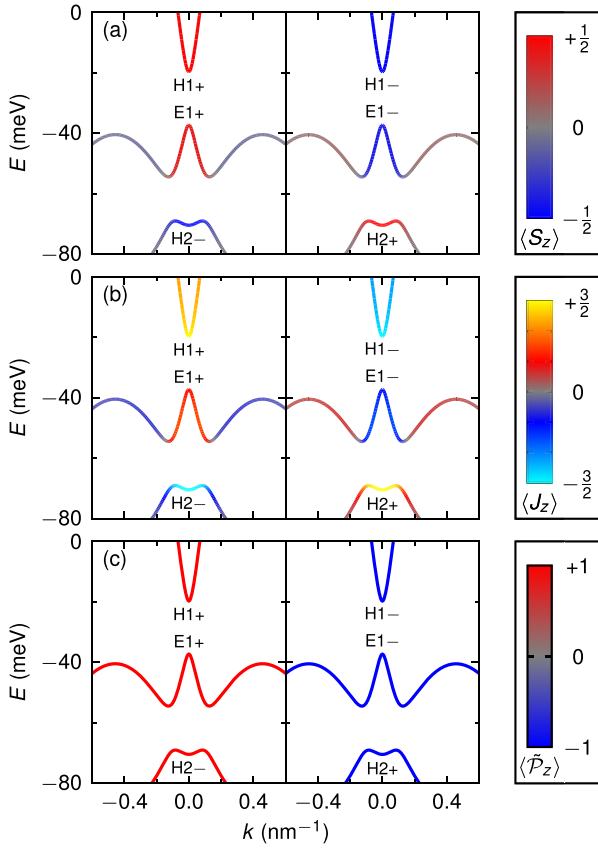
FIG. 1. Dispersion for a 7-nm HgTe quantum well between $Hg_{1-x}Cd_xTe$ ($x = 0.68$) barriers in the inversion-symmetric approximation. The momentum is parametrized as $(k_x, k_y) = k(1/\sqrt{2}, 1/\sqrt{2})$, along the (110) crystal direction. (a) Colors indicate spin expectation value $\langle S_z \rangle$. The visible subbands (labeled) belong to the same block; the states of the other block are degenerate, but not shown. (b) Same, with colors indicating $\langle J_z \rangle$. (c) Colors indicate $\langle \tilde{\mathcal{P}}_z \rangle$. We show the two degenerate copies of each state separately (left/right column), with the subbands grouped according to a six-band BHZ-type model [see Introduction and Eq. (4)].

The hybridization is strong enough that $\langle J_z \rangle$ changes sign at $k \approx 0.15$ nm^{-1}, as shown by the color of the band labeled E1+ in Fig. 1(b) changing from red to blue. Second, extension of the original four-band BHZ model with additional subbands cannot be done in a naive manner: For example, if one adds the second heavy-hole subbands $|H2, \pm\rangle$ to the "spin-up" and "spin-down" blocks of the four-band BHZ model, the two blocks are grouped [14,15]

$$\{|E1, +\rangle, |H1, +\rangle, |H2, -\rangle\},$$
$$\{|E1, -\rangle, |H1, -\rangle, |H2, +\rangle\}, \qquad (4)$$

where the H2 bands are in the opposite block from what one could naively expect. Thus, in extended BHZ-type models, one is no longer able to label the two blocks by 'spin' meaning $\langle \text{sgn}(J_z) \rangle$. Likewise, for the **k** · **p** model, containing many more degrees of freedom, this notion of "spin-up" and "spin-down" blocks cannot work properly. The notions of spin defined by S_z, J_z, and $\text{sgn}(J_z)$ not being good quantum numbers make them unsuitable for labeling the blocks.
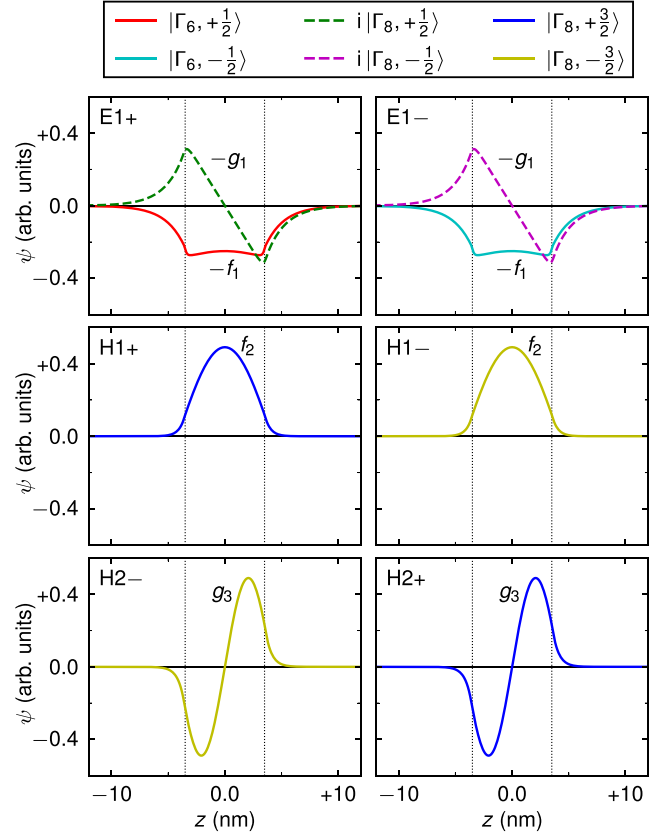

FIG. 2. Wave functions for the subbands $|E1, \pm\rangle$, $|H1, \pm\rangle$, and $|H2, \pm\rangle$ for a 7-nm HgTe quantum well at $(k_x, k_y) = (0, 0)$. The colors distinguish the orbital contributions. Zero and negligible contributions (among which the $|\Gamma_7, \pm\frac{1}{2}\rangle$ orbitals) are not shown. Solid and dashed curves denote the real and imaginary parts, respectively. The vertical dotted lines indicate the interfaces between quantum well (HgTe) and barriers ($Hg_{1-x}Cd_xTe$). We label the envelope functions f_i (even parity) and g_i (odd parity).

The particular grouping of the subband states given by Eq. (4) can be readily understood from their expansion into orbitals and envelope functions [15]

$$|E1, \pm\rangle = -f_1(z)|\Gamma_6, \pm\tfrac{1}{2}\rangle - ig_1(z)|\Gamma_8, \pm\tfrac{1}{2}\rangle,$$
$$|H1, \pm\rangle = f_2(z)|\Gamma_8, \pm\tfrac{3}{2}\rangle, \qquad (5)$$
$$|H2, \pm\rangle = g_3(z)|\Gamma_8, \pm\tfrac{3}{2}\rangle,$$

where the small contributions from $|\Gamma_7, \pm\frac{1}{2}\rangle$ have been neglected. The real functions f_i are even, g_i are odd under $z \to -z$ (see Fig. 2). The extended BHZ Hamiltonian thus groups states together which have either have identical spin and identical parity, or have opposite spin and opposite parity.

B. Isoparity

The fact that block-diagonal extensions of the BHZ model exist already hints at the possibility to find a similar block structure for the **k** · **p** model, from which the former is derived. The blocks are distinguished by a conserved quantum number; the previous observations suggest that it must involve both angular momentum and parity under the transformation

$|o\rangle$									$\langle o|Q|o\rangle$
$|\Gamma_6,+\tfrac{1}{2}\rangle$	E		E	O	E		O	E	+1
$|\Gamma_6,-\tfrac{1}{2}\rangle$		E		E	O	E	E	O	−1
$|\Gamma_8,+\tfrac{3}{2}\rangle$	E		E	O	E		O	E	+1
$|\Gamma_8,+\tfrac{1}{2}\rangle$	O	E	O	E	O	E	E	O	−1
$|\Gamma_8,-\tfrac{1}{2}\rangle$	E	O	E	O	E	O	O	E	+1
$|\Gamma_8,-\tfrac{3}{2}\rangle$		E		E	O	E	E	O	−1
$|\Gamma_7,+\tfrac{1}{2}\rangle$	O	E	O	E	O	E	E		−1
$|\Gamma_7,-\tfrac{1}{2}\rangle$	E	O	E	O	E	O		E	+1

FIG. 3. Parity structure of the Hamiltonian H_k and construction of the isoparity matrix Q. The labels "E" and "O" denote even and odd parity, respectively, under $P_z : z \to -z, k_z \to -k_z$, of the particular entry of the Hamiltonian. Even-parity entries contain even powers of k_z only (including constants), whereas odd-parity entries contain only odd powers. An empty position means that the matrix entry is identically zero. On the right-hand side, we indicate the diagonal matrix values $\langle o|Q|o\rangle$ for each of the orbitals $|o\rangle$ in the basis.

$z \to -z$. That is, the operator encoding this quantity should be the composition of the parity operation $P_z : z \mapsto -z, k_z \mapsto -k_z$ acting on spatial coordinates with a diagonal matrix Q in orbital space:

$$\tilde{\mathcal{P}}_z = P_z Q. \tag{6}$$

We name this operator *isoparity* because of its nature being a combination of spatial parity with another degree of freedom (spin).

The matrix Q in orbital space contains eigenvalues ± 1, such that opposite spins ($J_z = \pm m_J$) come with opposite signs. In order for the operator $\tilde{\mathcal{P}}_z$ to be a conserved quantity, $[H, \tilde{\mathcal{P}}_z] = 0$, it is required that Q satisfies

$$H^{\text{even}}Q = QH^{\text{even}} \quad \text{and} \quad H^{\text{odd}}Q = -QH^{\text{odd}}, \tag{7}$$

where the Hamiltonian $H = H^{\text{even}} + H^{\text{odd}}$ is separated into parts that are even and odd under the mirror operation P_z, i.e., containing even and odd powers of z or k_z, as indicated by the entries labeled "E" and "O" in Fig. 3. In other words, Q commutes (anticommutes) with the even (odd) part of the Hamiltonian under P_z. Thus, we find

$$Q = \text{diag}(+1, -1, +1, -1, +1, -1, -1, +1). \tag{8}$$

This matrix can simply be constructed by assigning the same diagonal value for all orbitals connected by even-parity matrix elements of the Hamiltonian, as shown in Fig. 3. This top-down construction of isoparity provides a suitable practical definition that is a conserved quantity by construction. In Sec. IV, we will provide a bottom-up derivation of this matrix from a fundamental perspective using representation theory of the crystallographic point group, that explains why it is conserved.

The conservation of isoparity in the $\mathbf{k} \cdot \mathbf{p}$ model is illustrated in Fig. 1(c) with dispersion curves colored according to the eigenstate expectation value $\langle \tilde{\mathcal{P}}_z \rangle$. Every eigenstate of the Hamiltonian is also an eigenstate of isoparity, with eigenvalue $\tilde{\mathcal{P}}_z = \pm 1$. The expectation values $\langle \tilde{\mathcal{P}}_z \rangle$ are consequently momentum independent: In the color coding of Fig. 1(c), states are either uniformly red or uniformly blue, indicating that they

have isoparity eigenvalue of $\tilde{\mathcal{P}}_z = +1$ and -1, respectively. In conclusion, the Hamiltonian admits a natural decomposition into two decoupled blocks defined by the isoparity eigenvalue.

Whereas we could also have chosen the opposite overall sign for Q, the definition of Eq. (8) intuitively connects to the blocks of the four-band BHZ model. The basis states $|E1, \pm\rangle$ and $|H1, \pm\rangle$ are eigenstates of isoparity with eigenvalues ± 1,

$$\tilde{\mathcal{P}}_z |E1, \pm\rangle = \pm |E1, \pm\rangle \quad \text{and} \quad \tilde{\mathcal{P}}_z |H1, \pm\rangle = \pm |H1, \pm\rangle. \tag{9}$$

The block quantum numbers defined by isoparity thus correspond to the $+$ and $-$ (or "up" and "down") labels for the blocks of the four-band BHZ model. For these four subband states, the isoparity eigenvalues happen to be equal to $\text{sgn}(J_z)$, but that is not generically true: For other subbands, the eigenvalues may be opposite, e.g., $\tilde{\mathcal{P}}_z |H2, \pm\rangle = \mp |H2, \pm\rangle$. Thus, the common interpretation of the two blocks as "spin blocks" is appropriate for the four-band BHZ model, but it breaks down for extended BHZ-type models. This observation underlines the need for the labeling to be defined unambiguously. Here, we use the conventional notation $+, -$ in terms of $\text{sgn}(J_z) = \pm 1$. The other choice would be for $+, -$ to mean the isoparity eigenvalue. If both $\tilde{\mathcal{P}}_z = \pm 1$ and $\text{sgn}(J_z) = \pm 1$ need to be considered, two distinct pairs of symbols need to be used, e.g., $\oplus, \ominus$ and $+, -$. The notation $\uparrow, \downarrow$ is discouraged.

C. Conservation laws

Let us verify invariance under isoparity $\tilde{\mathcal{P}}_z$, using the $\mathbf{k} \cdot \mathbf{p}$ Hamiltonian split into orbital blocks H_{pq}, as in Eq. (2). These blocks need to satisfy $H_{pq}^{\text{even}}Q_q = Q_p H_{pq}^{\text{even}}$ and $H_{pq}^{\text{odd}}Q_q = -Q_p H_{pq}^{\text{odd}}$, where $Q_6 = \text{diag}(+1, -1)$, $Q_8 = \text{diag}(+1, -1, +1, -1)$, and $Q_7 = \text{diag}(-1, +1)$ are the parts of Q [Eq. (8)] belonging to each orbital sector. We test these conditions for a selection of blocks H_{pq} explicitly, whereas the other conditions can be worked out along analogous lines. The blocks H_{pq} are written in a formal manner in Appendix A, following the notation of Ref. [11].

The diagonal blocks H_{66} and H_{77} are proportional to the identity matrix in the orbital basis, and thus automatically satisfy $H_{pp}^{\text{even}}Q_p = Q_p H_{pp}^{\text{even}}$. The block H_{88} [Eq. (A5)] contains a term proportional to the identity, as well as the two terms

$$\gamma_2\left[\left(J_x^2 - \tfrac{1}{3}J^2\right)k_x^2 + \left(J_y^2 - \tfrac{1}{3}J^2\right)k_y^2 + \left(J_z^2 - \tfrac{1}{3}J^2\right)k_z^2\right], \tag{10}$$

$$\gamma_3\left[\{J_x, J_y\}\{k_x, k_y\} + \{J_x, J_z\}\{k_x, k_z\} + \{J_y, J_z\}\{k_y, k_z\}\right], \tag{11}$$

where $J^2 = J_x^2 + J_y^2 + J_z^2$ and $\{A, B\} = AB + BA$ denotes the anticommutator. The γ_2 term is purely even in P_z, and commutes with Q_8 by virtue of $[J_i^2, Q_8] = 0$. For the γ_3 term, the even part is proportional to $\{k_x, k_y\}$, whereas $\{k_x, k_z\}$ and $\{k_y, k_z\}$ constitute the odd part. The identities $[\{J_x, J_y\}, Q_8] = 0$ and $\{\{J_i, J_z\}, Q_8\} = 0$ $(i = x, y)$ then provide invariance of this term under isoparity. The invariance of the off-diagonal blocks [Eqs. (A6)–(A8)] can be worked out in an analogous manner. Combining these results, we thus establish that H_k commutes with isoparity $\tilde{\mathcal{P}}_z$.

D. External fields: Magnetic, electric, and strain couplings

In order to describe realistic experimental settings, the Hamiltonian describing the band structure acquires several

terms related to external forces in addition to the purely momentum-dependent $\mathbf{k} \cdot \mathbf{p}$ Hamiltonian. Here, electric and magnetic fields are perhaps the first ones coming into mind, but also strain (in response to external stress) is of a similar nature.

Let us illustrate the implications of the field being intrinsic or external by the example of the Zeeman coupling acting on the Γ_6 orbitals,

$$H_{Z,6} = \mathbf{S} \cdot \mathbf{B} = S_x B_x + S_y B_y + S_z B_z \qquad (12)$$

$$= \frac{1}{2} \begin{pmatrix} B_z & B_x - iB_y \\ B_x + iB_y & -B_z \end{pmatrix}, \qquad (13)$$

where $\mathbf{S} = (S_x, S_y, S_z)$ is the spin operator and $\mathbf{B}$ the magnetic field. If we assume the magnetic field to be *intrinsic* (or if we consider the transformation to be a pure coordinate transformation), both $\mathbf{S}$ and $\mathbf{B}$ transform as axial vectors. For example, under P_z,

$$\begin{aligned} (S_x, S_y, S_z) &\rightarrow (-S_x, -S_y, S_z), \\ (B_x, B_y, B_z) &\rightarrow (-B_x, -B_y, B_z), \end{aligned} \qquad (14)$$

so that $\mathbf{S} \cdot \mathbf{B}$ is invariant. (The transformation of $\mathbf{S}$ follows from $S_i \rightarrow Q_6^\dagger S_i Q_6$.)

In contrast, if one considers the symmetry of the system subjected to an *external* magnetic field, then the latter should be considered as an external parameter that is unaffected by the transformation (or, in other words, transforms trivially), while $\mathbf{S}$, being intrinsic to the system, still transforms as an axial vector. Then we have

$$\begin{aligned} (S_x, S_y, S_z) &\rightarrow (-S_x, -S_y, S_z), \\ (B_x, B_y, B_z) &\rightarrow (B_x, B_y, B_z), \end{aligned} \qquad (15)$$

such that

$$H_{Z,6} \rightarrow Q_6^\dagger H_{Z,6} Q_6 = \frac{1}{2} \begin{pmatrix} B_z & -(B_x - iB_y) \\ -(B_x + iB_y) & -B_z \end{pmatrix}, \qquad (16)$$

i.e., $S_x B_x + S_y B_y + S_z B_z \rightarrow -S_x B_x - S_y B_y + S_z B_z$. The invariance of $\mathbf{S} \cdot \mathbf{B}$ is thus broken under this transformation if $B_x \neq 0$ or $B_y \neq 0$. Thus, the Zeeman-type term preserves isoparity if the field is perpendicular, $\mathbf{B} = (0, 0, B_z)$. For the Zeeman couplings in the other orbital sectors [11], the same conclusion follows analogously.

These observations keep their validity if the coupling is of the form $\mathbf{S} \cdot \mathbf{m}$, where $\mathbf{m}$ is a magnetic moment with the same transformation properties as $\mathbf{B}$. In particular, in $Hg_{1-x}Mn_xTe$, the exchange coupling couples the carrier spins to the (average) magnetic moments of the Mn ions. The response $\mathbf{m}(\mathbf{B})$ is paramagnetic [10], so that $\mathbf{m}$ transforms like $\mathbf{B}$. Thus, the magnetic couplings of HgTe and $Hg_{1-x}Mn_xTe$ have identical symmetry properties.

The magnetic field also modifies the $\mathbf{k} \cdot \mathbf{p}$ Hamiltonian following the Peierls substitution $\mathbf{k} \rightarrow \mathbf{k} + e\mathbf{A}/\hbar$, where $\mathbf{A}$ is the gauge potential, defined such that $\nabla \times \mathbf{A} = \mathbf{B}$. For isoparity to remain preserved, it is required that $\mathbf{A}$ transforms in a vectorlike manner under $P_z : z \rightarrow -z$, i.e., $(A_x, A_y, A_z) \rightarrow (A_x, A_y, -A_z)$, similar to the transformation of momentum $\mathbf{k}$. However, unlike momentum $\mathbf{k}$, the vector potential is defined with respect to the *external* magnetic field $\mathbf{B}$: Fixing

the gauge $\mathbf{A} = (-B_z y + B_y z, -B_x z, 0)$ and applying the transformation P_z, we find that $\mathbf{A}$ transforms to $\mathbf{A}' = (-B_z y - B_y z, B_x z, 0)$. The transformation $\mathbf{A} \rightarrow \mathbf{A}'$ is vectorlike exactly if the in-plane components vanish, $B_x = B_y = 0$. A nonzero out-of-plane component B_z preserves isoparity. Importantly, these conditions are identical to that of the Zeeman-type couplings. Consequently, isoparity remains a good quantum number in a perpendicular external magnetic field, but not if the in-plane components are nonzero.

An electric field (uniform in the in-plane coordinates x, y) can be modeled as an external potential $V(z)$ times the identity matrix $\mathbf{1}$ in the orbital basis. In view of condition (7), isoparity is preserved if

$$[V^{\text{even}}(z)\mathbf{1}, Q] = 0 \text{ and } \{V^{\text{odd}}(z)\mathbf{1}, Q\} = 0, \qquad (17)$$

where the function $V(z) = V^{\text{even}}(z) + V^{\text{odd}}(z)$ is split into even and odd parts under $z \rightarrow -z$. Thus, isoparity remains a good quantum number provided the odd part $V^{\text{odd}}(z)$ vanishes. It should be noted that the electric potential induced by a gate voltage has a nontrivial odd component, so that isoparity symmetry is broken. Consequently, the Rashba effect involves matrix elements off diagonal in isoparity (block quantum number). This result is well known in the context of BHZ [15,19], but thus also applies to the more generic setting of $\mathbf{k} \cdot \mathbf{p}$.

The deformation of the lattice as a result of matching the lattice constant to a substrate material is encoded as the rank-two symmetric strain tensor ϵ_{ij} [9,10]. Strain can be considered as the response to stress, the pressure applied to bring the lattice out of its equilibrium geometry. These forces are applied externally, and hence stress and strain must be treated as external fields. The strain Hamiltonian H^{str} describes the couplings between the orbitals and the strain tensor ϵ_{ij}. According to the formalism of Pikus and Bir, the possible couplings can be found from the $\mathbf{k} \cdot \mathbf{p}$ Hamiltonian by the substitutions $\frac{1}{2}\{k_i, k_j\} \rightarrow \epsilon_{ij}$ [9,10,18]. (See Appendix B for details.) As an external field, ϵ_{ij} transforms trivially, in contrast to $\{k_i, k_j\}$: whereas under parity in z, $\{k_x, k_z\}$ and $\{k_y, k_z\}$ are odd and $\{k_x, k_y\}$ and k_i^2 ($i = x, y, z$) are even, all components of ϵ_{ij} are even. From the invariance conditions of the $\mathbf{k} \cdot \mathbf{p}$ Hamiltonian derived above, we thus find that strain preserves isoparity if $\epsilon_{xz} = \epsilon_{yz} = 0$. This is the case for a material lattice strained to a substrate, where these shear strain components are typically assumed to vanish.

Figure 4 illustrates the effect of a magnetic field on isoparity on dispersions of the aforementioned quantum well in a strip geometry, 500 nm wide in the transversal direction $\hat{y}$ and translationally symmetric in the direction $\hat{x}$. This configuration models the devices used in experiments [1,13,23]. We have used the eight-orbital $\mathbf{k} \cdot \mathbf{p}$ model from Ref. [10]. We include strain from lattice matching the HgTe crystal to the lattice constant of the $Cd_{0.96}Zn_{0.04}Te$ substrate. The values of the coefficients are provided in Table II in the Appendix. The magnetic field is modeled by the Peierls substitution $\mathbf{k} \rightarrow \mathbf{k} + e\mathbf{A}/\hbar$ with the vector potential $\mathbf{A} = (-B_z y, 0, 0)$ in Landau gauge. For the confinement in $\hat{y}$ direction, we have used hard-wall boundary conditions. While a different choice of the boundary condition could affect the edge channel dispersion and the particular position of the Dirac point (the energy
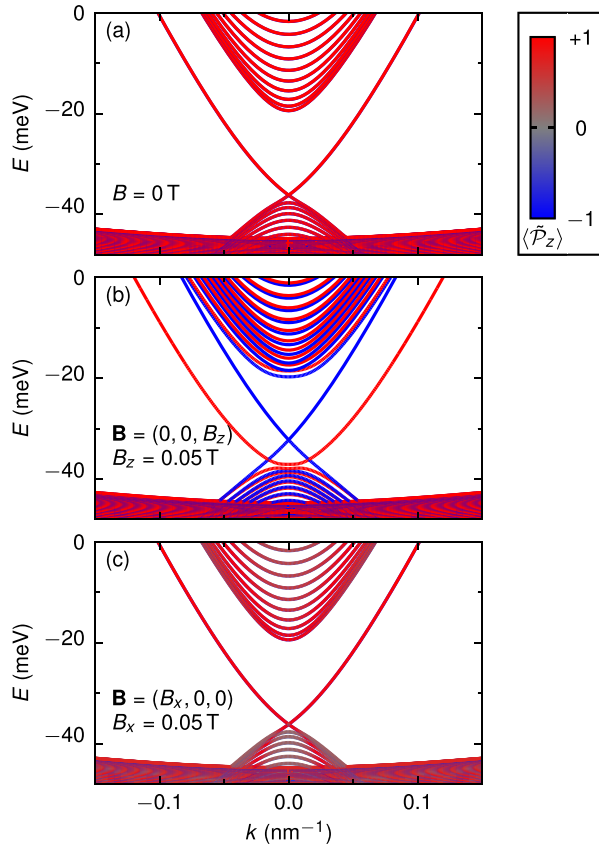
FIG. 4. Dispersion for the 7-nm HgTe quantum well in a strip geometry, 500 nm wide. (a) At zero field, $B = 0$, the eigenstates are degenerate, and can be separated into $\tilde{\mathcal{P}}_z = \pm 1$ states, as indicated by the color (see legend). (b) Dispersion for nonzero perpendicular field $\mathbf{B} = B_z \hat{z}$ with $B_z = 0.05$ T. (c) Dispersion for nonzero in-plane field $\mathbf{B} = B_x \hat{x}$ with $B_x = 0.05$ T.

where the dispersions cross) [24–26], it does not change the symmetry properties.

In absence of a magnetic field, the Hamiltonian eigenstates have block degeneracy; since $[H, \tilde{\mathcal{P}}_z] = 0$, all eigenstates can be classified as $\tilde{\mathcal{P}}_z = \pm 1$ [Fig. 4(a)]. In a finite perpendicular magnetic field $\mathbf{B} = B_z \hat{z}$ the block degeneracy is lifted, but each Hamiltonian eigenstate is still an eigenstate of $\tilde{\mathcal{P}}_z$ [Fig. 4(b)]. For an in-plane field $\mathbf{B} = B_x \hat{x}$, $\tilde{\mathcal{P}}_z$ no longer commutes with the Hamiltonian: In Fig. 4(c), we thus observe that the dispersion curves are colored nonuniformly, especially at the top of the valence band.

With the 'spin' of the edge channels being particularly important for spin transport, we can raise the question whether the existing interpretation of spin as $\text{sgn}(J_z) = \pm 1$ is adequate. In view of Eq. (9), the eigenvalues of $\text{sgn}(J_z)$ and $\tilde{\mathcal{P}}_z$ coincide for the $|E1, \pm\rangle$ and $|H1, \pm\rangle$ subband states. For the configurations of Figs. 4(a) and 4(b), the combined overlaps of each edge channel wave function with $|E1, \pm\rangle$ and $|H1, \pm\rangle$ are > 0.8 for all momenta $|k_x| \lesssim 0.1$ nm^{-1}. Thus, in the regime where the edge states cross the bulk gap, $\text{sgn}(J_z)$ may be used safely as a substitute for isoparity. Nonetheless, isoparity remains preferred in any configuration where it is an exactly conserved quantum number.

E. Inversion-symmetry breaking

For the $\mathbf{k} \cdot \mathbf{p}$ Hamiltonian, we have only included inversion-symmetric terms so far. Since the zinc-blende lattice structure does not possess inversion symmetry, the Hamiltonian may contain inversion-breaking terms. These are collectively known as bulk inversion asymmetry (BIA).

In order to demonstrate how BIA affects the block structure in the $\mathbf{k} \cdot \mathbf{p}$ Hamiltonian defined by isoparity, let us study the linear BIA term of the Γ_8 block [11],

$$H_{\text{BIA},C} = C_k \big[\{ J_x, J_y^2 - J_z^2 \} k_x + \{ J_y, J_z^2 - J_x^2 \} k_y$$
$$+ \{ J_z, J_x^2 - J_y^2 \} k_z \big]. \tag{18}$$

The k_x and k_y terms constitute the even part and the k_z term is the odd part. Using the definitions of the matrices J_i, we calculate

$$\{ \{ J_x, J_y^2 - J_z^2 \}, Q_8 \} = 0,$$
$$\{ \{ J_y, J_z^2 - J_x^2 \}, Q_8 \} = 0,$$
$$[\{ J_z, J_x^2 - J_y^2 \}, Q_8] = 0. \tag{19}$$

For the even and odd parts of the Hamiltonian, this yields

$$H^{\text{even}} Q = -Q H^{\text{even}} \quad \text{and} \quad H^{\text{odd}} Q = Q H^{\text{odd}}, \tag{20}$$

i.e., the even part anticommutes with Q (here, Q_8) while the odd part commutes, the opposite from the behavior of inversion-symmetric terms [see Eq. (7)]. Thus, we find that $H_{\text{BIA},C}$ anticommutes with isoparity,

$$H_{\text{BIA},C} \tilde{\mathcal{P}}_z = -\tilde{\mathcal{P}}_z H_{\text{BIA},C}. \tag{21}$$

The same property is valid for other bulk-inversion-asymmetric terms (see, e.g., Ref. [11]).

While the bulk-inversion antisymmetric terms are typically weaker than the symmetric terms [17], this is not generically valid for other inversion-asymmetric contributions. For example, structural inversion asymmetry (SIA) intrinsic to the geometry of the type-II heterostructure AlSb/InAs/GaSb/AlSb can be comparable to the topological gap [19]. Electrostatic gating can also induce asymmetries well above ∼10 meV.

Even if isoparity is not a symmetry, it may be useful to write the Hamiltonian in a basis of isoparity eigenstates. It then takes the form

$$H = \begin{pmatrix} H^+ & H_{\text{IA}} \\ H_{\text{IA}}^\dagger & H^- \end{pmatrix}, \tag{22}$$

where the blocks $H^\pm$ contain inversion-symmetric matrix elements of $\tilde{\mathcal{P}}_z = \pm 1$ states and H_{IA} contains the inversion-asymmetric terms. This structure is fully analogous to BHZ-type models in the basis $|E1, +\rangle$, $|H1, +\rangle$, $|E1, -\rangle$, $|H1, -\rangle$, where BIA and SIA terms appear in the off-diagonal block that couples $+$ and $-$ states [19,27]. Only if the off-diagonal blocks are small, isoparity is *weakly broken* and the inversion-asymmetric terms can be considered perturbatively.

IV. CRYSTAL SYMMETRY: POINT GROUP ANALYSIS

In the previous section, we have derived the isoparity operator $\tilde{\mathcal{P}}_z$ in an *a posteriori* manner, using invariance conditions with respect to a given Hamiltonian. In this section,

TABLE I. For each of the two-dimensional spinor subspaces in the top row, which together span the eight-orbital basis of the $\mathbf{k} \cdot \mathbf{p}$ model, the table provides: the angular momentum quantum numbers L, S, J, and m_J; the representation of the double point group $\tilde{D}_{4h}$ (Mulliken notation in parentheses); representation matrices $r(g)$ in for a selected subset of group elements g; the matrix θ of time reversal $T = \theta K$. We follow the conventions of the point group tables of Ref. [29].

Subspace	$\lvert \Gamma_6, \pm\frac{1}{2} \rangle$	$\lvert \Gamma_7, \pm\frac{1}{2} \rangle$	$\lvert \Gamma_8, \pm\frac{1}{2} \rangle$	$\lvert \Gamma_8, \pm\frac{3}{2} \rangle$
L	0	1	1	1
S	$\frac{1}{2}$	$\frac{1}{2}$	$\frac{1}{2}$	$\frac{1}{2}$
J	$\frac{1}{2}$	$\frac{1}{2}$	$\frac{3}{2}$	$\frac{3}{2}$
m_J	$\pm\frac{1}{2}$	$\pm\frac{1}{2}$	$\pm\frac{1}{2}$	$\pm\frac{3}{2}$
$\tilde{D}_{4h}$ rep.	$E_{1/2,g}(\bar{E}_{1g})$	$E_{1/2,u}(\bar{E}_{1u})$	$E_{1/2,u}(\bar{E}_{1u})$	$E_{3/2,u}(\bar{E}_{2u})$
m_z	$\begin{pmatrix} -i & 0 \\ 0 & i \end{pmatrix}$	$\begin{pmatrix} i & 0 \\ 0 & -i \end{pmatrix}$	$\begin{pmatrix} i & 0 \\ 0 & -i \end{pmatrix}$	$\begin{pmatrix} -i & 0 \\ 0 & i \end{pmatrix}$
m_x	$\begin{pmatrix} 0 & -i \\ -i & 0 \end{pmatrix}$	$\begin{pmatrix} 0 & i \\ i & 0 \end{pmatrix}$	$\begin{pmatrix} 0 & -i \\ -i & 0 \end{pmatrix}$	$\begin{pmatrix} 0 & -i \\ -i & 0 \end{pmatrix}$
m_y	$\begin{pmatrix} 0 & -1 \\ 1 & 0 \end{pmatrix}$	$\begin{pmatrix} 0 & 1 \\ -1 & 0 \end{pmatrix}$	$\begin{pmatrix} 0 & -1 \\ 1 & 0 \end{pmatrix}$	$\begin{pmatrix} 0 & 1 \\ -1 & 0 \end{pmatrix}$
TR θ	$\begin{pmatrix} 0 & -1 \\ 1 & 0 \end{pmatrix}$	$\begin{pmatrix} 0 & -1 \\ 1 & 0 \end{pmatrix}$	$\begin{pmatrix} 0 & 1 \\ -1 & 0 \end{pmatrix}$	$\begin{pmatrix} 0 & -1 \\ 1 & 0 \end{pmatrix}$

we will derive a suitable notion of block quantum number from the fundamental principles of crystal symmetries. Since the Hamiltonian is necessarily compatible with crystal symmetry, statements about invariance follow automatically, by construction.

The symmetries of the $\mathbf{k} \cdot \mathbf{p}$ model around $\mathbf{k} = \Gamma$ are described by one of the crystallographic point groups. The appropriate point group for unstrained bulk zinc-blende crystals is T_d (tetrahedral symmetry). If the system is confined and/or strained in the z direction, the point group is reduced to D_{2d}. Here, we consider the inversion-symmetric approximation; adding inversion to these groups, we obtain O_h and D_{4h}, respectively. In order to describe fermionic degrees of freedom, we need to extend these groups with the 2π rotation $\tilde{1}$. The resulting double covering groups are the *double point groups* $\tilde{O}_h$ and $\tilde{D}_{4h}$ [28].

We consider the transformations of the orbitals in the basis in Eq. (1). The four spin representations of the relevant double point group $\tilde{D}_{4h}$ are $E_{1/2,g}$, $E_{3/2,g}$, $E_{1/2,u}$, and $E_{3/2,u}$, where the subscripts $\frac{1}{2}$ and $\frac{3}{2}$ denote the quantum number m_J of the total angular momentum J_z and the subscripts g and u denote the parity under spatial inversion $I : (x, y, z) \to (-x, -y, -z)$, being *gerade* (even) and *ungerade* (odd), respectively. This parity corresponds to the orbital angular momentum L being an even or odd integer. We follow the notation used in the tables of Ref. [29], that is a slight modification of the common "Mulliken notation," used in Refs. [28,30,31] for example. The aforementioned four spin representations are written as $\bar{E}_{1g}$, $\bar{E}_{2g}$, $\bar{E}_{1u}$, and $\bar{E}_{2u}$, respectively, in the Mulliken notation.

In Table I, we list the orbitals of the $\mathbf{k} \cdot \mathbf{p}$ together with the angular momentum values L, S, and J (orbital, spin, and total, respectively) and m_J. From these values, we identify the appropriate spin representation. We subsequently provide the representation matrices $r(g)$ for several relevant group elements g: the mirrors m_i along the axes $i = x, y, z$. These representation matrices encode linear trans-

formation on the two-dimensional vector spaces with basis $\lvert \Gamma_p, +m_J \rangle$, $\lvert \Gamma_p, -m_J \rangle$ ($m_J > 0$), where the positive m_J is the first component. We have followed the conventions of the point group tables of Ref. [29], which we also recommend as a reference for additional information about this and other point groups. We remark that $\lvert \Gamma_7, \pm\frac{1}{2} \rangle$ and $\lvert \Gamma_8, \pm\frac{1}{2} \rangle$ transform both according to representation $E_{1/2,u}$, but the representation matrices are different, related by a unitary transformation.

The representation R for the eight-orbital $\mathbf{k} \cdot \mathbf{p}$ basis defined by Eq. (1) can simply be composed from those of the two-dimensional subspaces listed in Table I. Thus, the matrix $R(m_z)$ for m_z reads as

$$R(m_z) = \mathrm{diag}(-i, +i, -i, +i, -i, +i, +i, -i). \quad (23)$$

This matrix is identical to the matrix Q [Eq. (8)] for isoparity up to a factor: $R(m_z) = -iQ$. In view of the action of m_z on spatial quantities being given by P_z, we conclude that isoparity $\tilde{\mathcal{P}}_z$ is nothing else than the mirror operation in z up to the factor i. The two factors P_z and Q have a common origin, as the actions of m_z on the spatial and orbital degrees of freedom, respectively. This observation establishes why isoparity is conserved: the symmetry is of crystallographic origin. The transformations of the spinors follow naturally from the spin representations of the point group. By analogy, the matrices for $R(m_x)$ and $R(m_y)$ may be used to construct "in-plane isoparity."

V. TIME REVERSAL

Time reversal T acts differently on position and momentum $\mathbf{x} \to \mathbf{x}$ and $\mathbf{k} \to -\mathbf{k}$, respectively, as opposed to crystal symmetries where position and momentum transform in the same way. Consequently, time reversal also reverses angular momentum, including spin. Time reversal is required to be antiunitary in order the preserve the canonical quantization rules. In order to achieve these properties, time reversal is

typically realized as the combination $T = \theta K$ of a matrix θ in orbital space and complex conjugation, denoted K. For states with angular momentum J, this operator is most commonly represented by $\theta = \exp(-i\pi \hat{J}_y)$, itself a real matrix. The formal definition of time reversal requires the point group to be extended with time-reversed symmetry elements [32,33], but for the present case of crystals without magnetic ordering, it suffices to do the algebra by inserting complex conjugation K at the appropriate positions.

We specify the form of θ in all orbital subspaces of the $\mathbf{k} \cdot \mathbf{p}$ basis in Table I. In all four two-dimensional subspaces, $\theta = r(2_y) = \pm r(m_y)$, with $+$ and $-$ for *gerade* ($L = 0$) and *ungerade* ($L = 1$) representations, where 2_y denotes the π rotation around the y axis. From $r(2_y)r(m_z) = -r(m_z)r(2_y)$ and the fact that $r(m_z)$ is purely imaginary, it follows that time reversal commutes with m_z:

$$
\begin{aligned}
Tr(m_z) &= \theta K r(m_z) = -\theta r(m_z)K = r(m_z)\theta K \\
&= r(m_z)T.
\end{aligned}
\tag{24}
$$

Consequently, for a state belonging to one block, i.e., an eigenstate $|\Psi\rangle$ of $r(m_z)$ with $r(m_z)|\Psi\rangle = \pm i|\Psi\rangle$, we find that $r(m_z)T|\Psi\rangle = \mp iT|\Psi\rangle$, due to the complex conjugation in T.

Analogously, isoparity $\tilde{\mathcal{P}}_z$ anticommutes with time reversal T, so that for $|\Phi\rangle$ with $\tilde{\mathcal{P}}_z|\Phi\rangle = \pm|\Phi\rangle$, we have $\tilde{\mathcal{P}}_z T|\Phi\rangle = \mp T|\Phi\rangle$. Thus, the two members $|\Psi\rangle$ and $T|\Psi\rangle$ of a Kramers pair have opposite block quantum numbers. This property allows the interpretation of the two blocks as being Kramers partners. This fundamental idea, well known in the context the BHZ model, is also valid in the more generic $\mathbf{k} \cdot \mathbf{p}$ framework. As such, the division of the $\mathbf{k} \cdot \mathbf{p}$ Hamiltonian into isoparity subspaces $\tilde{\mathcal{P}}_z = \pm 1$ can be considered as a full generalization of the blocks in the BHZ model.

VI. MAGNETOTRANSPORT OBSERVABLES

While symmetry forces the transversal conductivity σ_{xy} to vanish at zero magnetic field, the salient feature of the quantum spin Hall effect is the presence of helical edge channels, that carry a spin Hall current. These edge channels come as a counterpropagating pair of Kramers partners. Their contributions $\sigma_{xy}^{\pm}$ to the Hall conductivity cancel out, $\sigma_{xy} = \sigma_{xy}^{+} + \sigma_{xy}^{-} = 0$, as to preserve the symmetry relation $\sigma_{xy} = 0$. On the other hand, the difference $\tilde{\sigma}_{xy} = \sigma_{xy}^{+} - \sigma_{xy}^{-}$ is not required to vanish. The two partners being related by time reversal, they can be interpreted as two states with opposite spin, and one can thus call $\tilde{\sigma}_{xy}$ the spin Hall conductivity [34].

With the interpretation of the blocks $\tilde{\mathcal{P}}_z = \pm 1$ as Kramers partners, we can utilize isoparity to generalize the concept of spin conductance to the $\mathbf{k} \cdot \mathbf{p}$ framework: The difference between the conductivity tensor associated to either block is simply a composition of the conductivity tensor σ with the isoparity operator $\tilde{\mathcal{P}}_z$,

$$
\tilde{\sigma}_{ij} = \sigma_{ij}\tilde{\mathcal{P}}_z.
\tag{25}
$$

While ordinary conductivity σ satisfies Ohm's law $\mathbf{j} = \sigma\mathbf{E}$, spin conductivity satisfies the analogous equation $\tilde{\mathbf{j}} = \tilde{\sigma}E$, involving the *spin current* $\tilde{\mathbf{j}} = \mathbf{j}\tilde{\mathcal{P}}_z$, that can be viewed in terms of two types of carriers with opposite charge depending on the isoparity eigenvalue.

The transformation rules of σ and $\tilde{\sigma}$ under mirror symmetries readily follow from the group-theoretical analysis of Sec. IV: isoparity $\tilde{\mathcal{P}}_z = im_z$ commutes with m_z and anticommutes with m_x and m_y. Under the latter two transformations, spin conductivity $\tilde{\sigma}$ obtains an opposite sign compared to charge conductivity σ, so that

$$
\sigma_{xy}(-B_z) = -\sigma_{xy}(B_z), \quad \tilde{\sigma}_{xy}(-B_z) = \tilde{\sigma}_{xy}(B_z).
\tag{26}
$$

Unlike the ordinary Hall conductivity σ_{xy}, the spin Hall conductivity $\tilde{\sigma}_{xy}$ is not required to vanish at zero magnetic field. In other words, spin Hall conductivity may be nonzero at zero magnetic field, which makes the existence of helical counterpropagating edge channels possible.

The transformation of transport tensors L_{ij} under time reversal T is subject to the principle of Onsager's relation [20,21]

$$
L_{ij}(\mathbf{S}, \mathbf{B}) = L_{ji}(-\mathbf{S}, -\mathbf{B}),
\tag{27}
$$

where $\mathbf{S}$ encodes the spin configuration of the system. The key property of $\mathbf{S}$ is that $\mathbf{S} \to -\mathbf{S}$ under time reversal. Here, isoparity plays this role. The conductivity contributions $\sigma_{ij}^{\pm}$ from the isoparity blocks $\tilde{\mathcal{P}}_z = \pm 1$ thus satisfy

$$
\sigma_{ij}^{\pm}(\mathbf{B}) = \sigma_{ji}^{\mp}(-\mathbf{B}).
\tag{28}
$$

(We note that in Chern insulator models with a single spin or isoparity block, see Refs. [22,35] for example, there is no such relation.) For the ordinary conductivity $\sigma_{ij} = \sigma_{ij}^{+} + \sigma_{ij}^{-}$, the symmetric $\sigma_{ij}^{s} = \frac{1}{2}(\sigma_{ij} + \sigma_{ji})$ and antisymmetric $\sigma_{ij}^{a} = \frac{1}{2}(\sigma_{ij} - \sigma_{ji})$ parts are even and odd under time reversal, respectively,

$$
\sigma_{ij}^{s}(-\mathbf{B}) = \sigma_{ij}^{s}(\mathbf{B}), \quad \sigma_{ij}^{a}(-\mathbf{B}) = -\sigma_{ij}^{a}(\mathbf{B}).
\tag{29}
$$

In contrast, spin conductivity $\tilde{\sigma}_{ij} = \sigma_{ij}^{+} - \sigma_{ij}^{-}$ obtains opposite signs compared to σ_{ij},

$$
\tilde{\sigma}_{ij}^{s}(-\mathbf{B}) = -\tilde{\sigma}_{ij}^{s}(\mathbf{B}), \quad \tilde{\sigma}_{ij}^{a}(-\mathbf{B}) = \tilde{\sigma}_{ij}^{a}(\mathbf{B}).
\tag{30}
$$

The opposite signs originate in the isoparity component $\tilde{\mathcal{P}}_z$ [see Eq. (25)], which anticommutes with time reversal.

For $\mathbf{B} = 0$, Eqs. (29) and (30) thus express the idea that time reversal forces Hall conductivity σ_{xy} to vanish while spin Hall conductivity $\tilde{\sigma}_{xy}$ may be finite. For finite magnetic fields $\mathbf{B} \neq 0$, Onsager's relation merely connects the two opposite isoparity blocks at $\mathbf{B}$ and $-\mathbf{B}$. The values $\sigma_{xy}^{+}(\mathbf{B})$ and $\sigma_{xy}^{-}(\mathbf{B})$ are independent and may be finite, which permits the quantum Hall effect as well as the quantum anomalous Hall effect [36]. We conclude from this discussion that the concepts and properties of these transport tensors known from the BHZ formalism extend to $\mathbf{k} \cdot \mathbf{p}$. The key property of isoparity that accommodates this generalization is the idea that the isoparity sectors are Kramers partners.

VII. CONCLUSION AND DISCUSSION

The term *quantum spin Hall effect* is more subtle than it appears at first sight: The effect pairs a zero total Hall conductivity with a nonzero spin Hall conductivity, being the sum and difference, respectively, of contributions from two 'spin' states. Here, we have demonstrated that these two 'spin' states are neither proper spin S_z nor total angular momentum

J_z, but the eigenvalues of the mirror transformation m_z or the equivalent observable that we dubbed *isoparity* $\tilde{\mathcal{P}}_z$. The block structure of the Hamiltonian is defined by the quantum numbers defined by m_z or $\tilde{\mathcal{P}}_z$ (values are $\pm i$ or ± 1, respectively). The conservation of these quantities naturally follows from crystal symmetries. The key property that makes isoparity "behave like spin" is the fact that it anticommutes with time reversal. As time reversal maps the $\tilde{\mathcal{P}}_z = +1$ subspace to the $\tilde{\mathcal{P}}_z = -1$ subspace, they constitute Kramers partners, analogous to the same idea in the BHZ model framework. Thus, by analogy, spin conductivity is defined as the transport tensor $\tilde{\sigma}_{ij} = \sigma_{ij}\tilde{\mathcal{P}}_z$, defined by combining ordinary conductivity tensor σ_{ij} with isoparity. These analogies establish the isoparity subspaces as a complete generalization of the notion of the block structure of the BHZ model. In conclusion, while 'spin' in "quantum spin Hall" should be more accurately understood as isoparity, the analogy justifies the colloquial usage of the word 'spin.'

The conservation of isoparity requires m_z to be a crystal symmetry, which is, however, not contained in the point group $\tilde{T}_d$ of (unstrained bulk) zinc-blende materials. The block structure can thus be defined by isoparity only in the inversion-symmetric approximation: By neglecting inversion-asymmetric terms, the point group is enlarged to $\tilde{O}_h$, or one of its subgroups that contain inversion. While actual topological insulator devices are often not symmetric under $z \rightarrow -z$, modeling of the band structures in the inversion-symmetric approximation (including BHZ-type models) is ubiquitous in literature. Even in absence of this symmetry, a basis of isoparity eigenstates may be chosen. This will lead to a block structure of the Hamiltonian with isoparity-preserving terms in the diagonal blocks, and the isoparity-breaking terms in the off-diagonal blocks, again in full analogy to the BHZ model. A perturbative treatment of the symmetry-breaking terms is possible if they are sufficiently small.

In practice, the isoparity operator can be applied in **k · p** numerics in order to lift degeneracy between the blocks, by addition of a small term $\epsilon\tilde{\mathcal{P}}_z$ to the Hamiltonian. Whereas one could successfully lift degeneracy with diagonal operators like ϵJ_z or $\epsilon \, \text{sgn}(J_z)$, these have the disadvantage that they do not constitute conserved quantum numbers. In fact, we have demonstrated that the expectation values $\langle J_z \rangle$ can change signs at larger momentum values, which leads to accidental crossings, that complicates the study of the properties of single bands. These issues are avoided if the lifting term is given by the conserved quantity $\tilde{\mathcal{P}}_z$. Despite the operator $\tilde{\mathcal{P}}_z$ being nondiagonal, it can be implemented conveniently and efficiently in sparse-matrix form.

ACKNOWLEDGMENTS

of Fig. 4 were performed at the Julia-HPC high-performance-computing cluster at the University of Würzburg.

APPENDIX A: INVERSION-SYMMETRIC k · p HAMILTONIAN

The inversion-symmetric **k · p** Hamiltonian H_k is split into orbital blocks H_{pq} ($p, q = 6, 7, 8$) according to Eq. (2). (We drop the subscript k in the orbital block notation.) We provide an abstract notation in terms of angular momentum matrices [11]. The latter notation is especially convenient for testing invariance. The explicit matrix forms can be found in Refs. [9–11], for example, or from substitution of the angular momentum matrices.

For the diagonal blocks, the relevant angular momentum matrices are the 2×2 Pauli matrices

$$\sigma_x = \begin{pmatrix} 0 & 1 \\ 1 & 0 \end{pmatrix}, \quad \sigma_y = \begin{pmatrix} 0 & -i \\ i & 0 \end{pmatrix}, \quad \sigma_z = \begin{pmatrix} 1 & 0 \\ 0 & -1 \end{pmatrix}, \tag{A1}$$

and the 4×4 $J = \frac{3}{2}$ angular momentum matrices

$$J_x = \begin{pmatrix} 0 & \theta & 0 & 0 \\ \theta & 0 & 1 & 0 \\ 0 & 1 & 0 & \theta \\ 0 & 0 & \theta & 0 \end{pmatrix}, \quad J_y = i\begin{pmatrix} 0 & -\theta & 0 & 0 \\ \theta & 0 & -1 & 0 \\ 0 & 1 & 0 & -\theta \\ 0 & 0 & \theta & 0 \end{pmatrix},$$

$$J_z = \begin{pmatrix} \frac{3}{2} & 0 & 0 & 0 \\ 0 & \frac{1}{2} & 0 & 0 \\ 0 & 0 & -\frac{1}{2} & 0 \\ 0 & 0 & 0 & -\frac{3}{2} \end{pmatrix}, \tag{A2}$$

with $\theta = \frac{1}{2}\sqrt{3}$, as well as the respective identity matrices. The diagonal blocks of H_k are

$$H_{66} = \left(E_6 + \frac{\hbar^2}{2m'}k^2\right)\mathbf{1}_{2\times 2}, \tag{A3}$$

$$H_{77} = \left(E_7 - \frac{\hbar^2}{2m_0}\gamma_1 k^2\right)\mathbf{1}_{2\times 2}, \tag{A4}$$

and

$$\begin{aligned} H_{88} = {} & \left(E_8 - \frac{\hbar^2}{2m_0}\gamma_1 k^2\right)\mathbf{1}_{4\times 4} + \frac{\hbar^2}{2m_0}2\gamma_2\left[\left(J_x^2 - \frac{1}{3}J^2\right)k_x^2\right. \\ & + \left(J_y^2 - \frac{1}{3}J^2\right)k_y^2 + \left(J_z^2 - \frac{1}{3}J^2\right)k_z^2\right] \\ & + \frac{\hbar^2}{2m_0}\gamma_3[\{J_x, J_y\}\{k_x, k_y\} + \{J_x, J_z\}\{k_x, k_z\} \\ & + \{J_y, J_z\}\{k_y, k_z\}], \end{aligned} \tag{A5}$$

where $J^2 = J_x^2 + J_y^2 + J_z^2$ and $k^2 = k_x^2 + k_y^2 + k_z^2$, E_p ($p = 6, 7, 8$) are the energies of the band edges at $k = 0$, m_0 is the electron mass, m' is the Γ_6 effective mass, and $\gamma_{1,2,3}$ are the Luttinger parameters [9,11]. The curly brackets denote the anticommutator $\{A, B\} = AB + BA$. The off-diagonal blocks are

$$H_{67} = -\frac{1}{3}\sqrt{3}P(\sigma_x k_x + \sigma_y k_y + \sigma_z k_z), \tag{A6}$$

$$H_{68} = -\sqrt{3}P(T_x k_x + T_y k_y + T_z k_z), \tag{A7}$$

TABLE II. Coefficients of the inversion-symmetric $\mathbf{k} \cdot \mathbf{p}$ Hamiltonian H_k and the strain Hamiltonian H^{str}. The values are adapted from Refs. [9,10], with values for HgTe provided as is, and those for $\text{Hg}_{0.32}\text{Cd}_{0.68}\text{Te}$ obtained from interpolation between HgTe and CdTe.

	E_6 (meV)	E_7 (meV)	E_8 (meV)	m'/m_0	P (meV nm)	γ_1	γ_2	γ_3	C (eV)	a (eV)	b (eV)	d (eV)	$\epsilon_\parallel$ (10^{-3})	$\epsilon_\perp$ (10^{-3})
HgTe	-303	-1080	0	1	846	4.1	0.50	1.30	-3.83	0.00	-1.50	-2.08	0.76	-1.04
$\text{Hg}_{0.32}\text{Cd}_{0.68}\text{Te}$	587	-1343	-379	1.14	846	2.3	-0.02	0.43	-3.99	-0.48	-1.26	-2.44	-1.11	1.54

$$H_{78} = \frac{\hbar^2}{2m_0} 6\gamma_2 \left(T_{xx} k_x^2 + T_{yy} k_y^2 + T_{zz} k_z^2 \right)$$
$$+ \frac{\hbar^2}{2m_0} 6\gamma_3 (T_{xy}\{k_x, k_y\} + T_{yz}\{k_y, k_z\} + T_{zx}\{k_z, k_x\})$$
$$\text{(A8)}$$

in terms of the 2×4 angular momentum matrices T_i and T_{ij} ($i, j = 1, 2, 3$; see Ref. [11]), the Kane matrix element $P = -(\hbar/m_0)\langle S|p_x|X\rangle$ [7], and the Luttinger parameters $\gamma_{2,3}$.

The dispersions and wave functions of Figs. 1 and 2 have been calculated in a layer stack geometry with a 7-nm HgTe quantum well between barriers of $\text{Hg}_{1-x}\text{Cd}_x\text{Te}$ with $x = 0.68$. The thickness of the barriers in the simulation is 10 nm, sufficient for the wave functions to decay. In this geometry, there is no translational symmetry in the z direction. The appropriate Hamiltonian in this geometry has the form $H(k_x, k_y, z)$ and is obtained from the bulk Hamiltonian $H(k_x, k_y, k_z)$ by the substitution $k_z \rightarrow -i\partial_z$. The coefficients of the $\mathbf{k} \cdot \mathbf{p}$ Hamiltonian being material dependent, they are realized as piecewise constant functions of z with smooth interpolation near the interface. The values for HgTe [10] and $\text{Hg}_{1-x}\text{Cd}_x\text{Te}$ at $x = 0.68$ are summarized in Table II.

The z coordinate is discretized in steps of 0.25 nm. The resulting Hamiltonian $H(k_x, k_y)$ has dimensions $N \times N$ with $N = 8n_z$, where n_z is the number of discrete coordinates in the z direction. The dispersions $E_n(k_x, k_y)$ are obtained by numerical diagonalization of this matrix. The wave functions and expectation values ($\langle S_z \rangle$, $\langle J_z \rangle$, etc.) are extracted from the eigenstates. In the strip calculation of Fig. 4, the Hamiltonian $H(k_x, y, z)$ is discretized additionally in the y direction. This leads to a Hamiltonian matrix $H(k_x)$ of dimension $N \times N$ with $N = 8n_z n_y$, where n_y is the number of discrete coordinates in the y direction. In view of the large matrix sizes, diagonalization has been performed with sparse matrix methods at a high-performance-computing infrastructure with a high degree of parallelization.

APPENDIX B: STRAIN HAMILTONIAN

The uniaxial strain induced by lattice matching of the materials to the substrate is modeled by the Pikus-Bir strain Hamiltonian H^{str} in terms of the strain tensor ϵ_{ij} ($i, j = x, y, z$) [18]. In the Pikus-Bir formalism, the strain Hamiltonian is obtained by substitution of quadratic momenta $\frac{1}{2}\{k_i, k_j\} \rightarrow \epsilon_{ij}$ from the $\mathbf{k} \cdot \mathbf{p}$ Hamiltonian H_k. The coefficients of the terms are the deformation potentials C, a, b, and d [9,10]. (Other notations are common, e.g., $C_1 = C$, $D_d = a$, $D_u = -\frac{3}{2}b$, and $D_u' = -\frac{1}{2}\sqrt{3}d$ in Ref. [11].) The values provided in Table II are extracted from Ref. [9].

The substitution from H_k yields the diagonal blocks

$$H_{66}^{\text{str}} = C \operatorname{tr}\epsilon \, \mathbf{1}_{2\times 2}, \tag{B1}$$

$$H_{77}^{\text{str}} = a \operatorname{tr}\epsilon \, \mathbf{1}_{2\times 2}, \tag{B2}$$

$$H_{88}^{\text{str}} = a\operatorname{tr}\epsilon \, \mathbf{1}_{4\times 4} - b\left[\left(J_x^2 - \frac{1}{3}J^2 \right)\epsilon_{xx} \right.$$
$$+ \left(J_y^2 - \frac{1}{3}J^2 \right)\epsilon_{yy} + \left(J_z^2 - \frac{1}{3}J^2 \right)\epsilon_{zz} \left. \right]$$
$$- \frac{d}{\sqrt{3}}[\{J_x, J_y\}\epsilon_{xy} + \{J_x, J_z\}\epsilon_{xz} + \{J_y, J_z\}\epsilon_{yz}], \tag{B3}$$

with $\operatorname{tr}\epsilon = \epsilon_{xx} + \epsilon_{yy} + \epsilon_{zz}$. Furthermore, we have the off-diagonal block

$$H_{78}^{\text{str}} = -3b(T_{xx}\epsilon_{xx} + T_{yy}\epsilon_{yy} + T_{zz}\epsilon_{zz})$$
$$- \sqrt{3}d(T_{xy}\epsilon_{xy} + T_{yz}\epsilon_{yz} + T_{zx}\epsilon_{zx}). \tag{B4}$$

The off-diagonal blocks H_{68}^{str} and H_{67}^{str} vanish as the corresponding blocks of H_k do not contain terms of quadratic or higher order in k (under the assumption of inversion symmetry).

The strain tensor ϵ_{ij} is determined by matching the in-plane lattice constants of the quantum-well and barrier layers are matched to the lattice constant 0.6467 nm of the $\text{Cd}_{0.96}\text{Zn}_{0.04}\text{Te}$ substrate. The equilibrium lattice constants for HgTe (quantum well) and $\text{Hg}_{0.32}\text{Cd}_{0.68}\text{Te}$ (barrier) are 0.6462 and 0.6474 nm, respectively. This leads to a strain tensor $\epsilon = \operatorname{diag}(\epsilon_\parallel, \epsilon_\parallel, \epsilon_\perp)$ with $\epsilon_\parallel$ and $\epsilon_\perp$ given in Table II.

[1] M. König, S. Wiedmann, C. Brüne, A. Roth, H. Buhmann, L. W. Molenkamp, X.-L. Qi, and S.-C. Zhang, Science **318**, 766 (2007).

[2] C. Brüne, C. X. Liu, E. G. Novik, E. M. Hankiewicz, H. Buhmann, Y. L. Chen, X. L. Qi, Z. X. Shen, S. C. Zhang, and L. W. Molenkamp, Phys. Rev. Lett. **106**, 126803 (2011).

[3] C. L. Kane and E. J. Mele, Phys. Rev. Lett. **95**, 146802 (2005).

[4] B. A. Bernevig, T. L. Hughes, and S.-C. Zhang, Science **314**, 1757 (2006).

[5] D. J. Thouless, M. Kohmoto, M. P. Nightingale, and M. den Nijs, Phys. Rev. Lett. **49**, 405 (1982).

[6] A. Roth, C. Brüne, H. Buhmann, L. W. Molenkamp, J. Maciejko, X.-L. Qi, and S.-C. Zhang, Science **325**, 294 (2009).

[7] E. O. Kane, J. Phys. Chem. Solids **1**, 249 (1957).

[8] M. H. Weiler, in *Defects, (HgCd)Se, (HgCd)Te*, Semiconductors and Semimetals, Vol. 16, edited by R. K. Willardson and A. C. Beer (Academic, New York, 1981), Chap. 3, pp. 119–191.

[9] A. Pfeuffer-Jeschke, Ph.D. thesis, Würzburg University, Würzburg, Germany, 2000.

[10] E. G. Novik, A. Pfeuffer-Jeschke, T. Jungwirth, V. Latussek, C. R. Becker, G. Landwehr, H. Buhmann, and L. W. Molenkamp, Phys. Rev. B **72**, 035321 (2005).

[11] R. Winkler, *Spin Orbit Coupling Effects in Two-dimensional Electron and Hole systems* (Springer, Berlin, 2003).

[12] K. Ortner, X. C. Zhang, A. Pfeuffer-Jeschke, C. R. Becker, G. Landwehr, and L. W. Molenkamp, Phys. Rev. B **66**, 075322 (2002).

[13] S. Shamim, W. Beugeling, J. Böttcher, P. Shekhar, A. Budewitz, P. Leubner, L. Lunczer, E. M. Hankiewicz, H. Buhmann, and L. W. Molenkamp, Sci. Adv. **6**, eaba4625 (2020).

[14] S. S. Krishtopenko and F. Teppe, Phys. Rev. B **97**, 165408 (2018).

[15] D. G. Rothe, R. W. Reinthaler, C.-X. Liu, L. W. Molenkamp, S.-C. Zhang, and E. M. Hankiewicz, New J. Phys. **12**, 065012 (2010).

[16] L. C. Andreani, A. Pasquarello, and F. Bassani, Phys. Rev. B **36**, 5887 (1987).

[17] M. Orlita, K. Masztalerz, C. Faugeras, M. Potemski, E. G. Novik, C. Brüne, H. Buhmann, and L. W. Molenkamp, Phys. Rev. B **83**, 115307 (2011).

[18] G. L. Bir and G. E. Pikus, *Symmetry and Strain-induced Effects in Semiconductors* (Wiley, Chichester, 1974).

[19] C.-X. Liu, T. L. Hughes, X.-L. Qi, K. Wang, and S.-C. Zhang, Phys. Rev. Lett. **100**, 236601 (2008).

[20] H. Grimmer, Acta Crystallogr. A **49**, 763 (1993).

[21] H. Grimmer, Acta Crystallogr. A **73**, 333 (2017).

[22] J. Böttcher, C. Tutschku, and E. M. Hankiewicz, Phys. Rev. B **101**, 195433 (2020).

[23] S. Shamim, P. Shekhar, W. Beugeling, J. Böttcher, A. Budewitz, J.-B. Mayer, L. Lunczer, E. M. Hankiewicz, H. Buhmann, and L. W. Molenkamp (unpublished).

[24] O. E. Raichev, Phys. Rev. B **85**, 045310 (2012).

[25] R. Skolasinski, D. I. Pikulin, J. Alicea, and M. Wimmer, Phys. Rev. B **98**, 201404(R) (2018).

[26] P. C. Klipstein, arXiv:2011.05720.

[27] M. König, H. Buhmann, L. W. Molenkamp, T. Hughes, C.-X. Liu, X.-L. Qi, and S.-C. Zhang, J. Phys. Soc. Jpn **77**, 031007 (2008).

[28] L. Elcoro, B. Bradlyn, Z. Wang, M. G. Vergniory, J. Cano, C. Felser, B. A. Bernevig, D. Orobengoa, G. de la Flor, and M. I. Aroyo, J. Appl. Crystallogr. **50**, 1457 (2017).

[29] S. L. Altmann and P. Herzig, *Point-group Theory Tables*, Oxford Science publications, 2nd ed. (corrected) (Clarendon, Oxford, 1994).

[30] R. S. Mulliken, Phys. Rev. **43**, 279 (1933).

[31] C. J. Bradley and A. P. Cracknell, *Mathematical Theory of Symmetry in Solids: Representation Theory for Point Groups and Space Groups* (Clarendon, Oxford, United Kingdom, 1972).

[32] L. D. Landau and E. M. Lifshitz, *Statistical Physics*, Course of Theoretical Physics, Vol. 5 (Pergamon, Oxford, United Kingdom, 1985).

[33] B. A. Tavger and V. M. Zaitsev, Zh. Eksp. Teor. Fiz. **30**, 564 (1956) [Sov. Phys.–JETP **3**, 430 (1956)].

[34] B. A. Bernevig and S.-C. Zhang, Phys. Rev. Lett. **96**, 106802 (2006).

[35] J. Böttcher, C. Tutschku, L. W. Molenkamp, and E. M. Hankiewicz, Phys. Rev. Lett. **123**, 226602 (2019).

[36] C.-X. Liu, X.-L. Qi, X. Dai, Z. Fang, and S.-C. Zhang, Phys. Rev. Lett. **101**, 146802 (2008).